Journal of Applied Physics METHOD scitation.org/journal/jap

A two-sensor 3ω-2ω method for thermal boundary resistance measurement

Cite as: J. Appl. Phys. 129, 125107 (2021); doi: 10.1063/5.0039444
Submitted: 3 December 2020 · Accepted: 4 March 2021 ·
Published Online: 26 March 2021

Yu-Chao Hua and Bing-Yang Cao[a)]

AFFILIATIONS

Key Laboratory for Thermal Science and Power Engineering of Ministry of Education, Department of Engineering Mechanics, Tsinghua University, Beijing 100084, People's Republic of China

[a)]Author to whom correspondence should be addressed: caoby@mail.tsinghua.edu.cn

ABSTRACT

Thermal boundary resistance (TBR), which measures an interface's resistance to the thermal flow, is of critical importance among various areas, such as electronics cooling and thermoelectric materials. As for measuring TBR, electrical techniques are generally less sensitive compared to optical ones, but they are easily operable and compatible with the measurement of other electric properties; thus, it is highly desirable to develop electrical methods with higher accuracy and larger measurement range. Here, a two-sensor 3ω-2ω method with a novel experimental procedure design is proposed, which can well address those deficiencies in the conventional 3ω method. Two parallel metal sensors are fabricated, with one of them being wide and the other being narrow. The temperature changes of these two sensors are measured by detecting the 3ω and 2ω signals, respectively. The measurement includes three steps: (1) obtain thin film's thermal conductivity from the wide sensor's 3ω thermal response; (2) obtain substrate thermal conductivity from the narrow sensor's 2ω thermal response; and (3) derive an effective TBR from the narrow sensor's 3ω thermal response. Moreover, it is found the TBRs of metal/dielectric and dielectric/substrate interfaces are distinguishable due to the considerable difference between their contact areas, which enables us to separate these two TBRs by varying the contact area (heater's width). Then, our method is employed to probe the TBRs between the Al_2O_3 nanofilm and Si as well as SiC substrates at room temperature and good agreement with the previous measurements is achieved, verifying its feasibility. Our present scheme will be helpful for the experimental study of interfacial thermal transport.

I. INTRODUCTION

Thermal boundary resistance (TBR) is playing a crucial role in modern technologies, including electronics cooling and design of advanced thermal-functional materials. With the rapid miniaturization of electronic devices, the density of material interfaces is dramatically increasing, which makes interfacial thermal transport a dominant factor for the overall thermal performance.[1–3] The utilization of high-thermal-conductivity substrate materials further intensifies the influence of TBR. As an example, in a GaN-on-diamond transistor, the TBR between the GaN layer and the diamond substrate, which is equal to about 27 m^2K/GW, can account for approximately 40% of the total thermal resistance.[4] In addition, TBR is of importance for developing nanostructured thermal functional materials.[5,6] To obtain a material of high thermoelectric figure of merit requires reducing its lattice thermal conductivity to be as low as possible, and increasing TBR (such as superlattice structures) is an efficient way to achieve this goal;[5] on the contrary, reducing TBR is the key to fabricate graphene-based thermal interface materials of high thermal conductivity.[6] Therefore, the investigation of TBR has drawn much attention from researchers in the communities of electronics, thermal, and material sciences.[7–9]

Experimental characterization provides fundamental data for studying TBR. Table I summarizes the measurement techniques that have been used to probe TBR at small scale, with a comparison between them. Ultrafast laser-based transient thermoreflectance (TTR) methods,[10] including TDTR (time-domain thermoreflectance) and FDTR (frequency-domain thermoreflectance), have been widely used to measure the TBR between nanofilms.[11–16] Due to the modulated pump laser's ultrahigh frequency that can reach 10 MHz and thus the small thermal penetration length, the detected signals (i.e., the phase angles between in-plane and out-plane signals) in TTR experiments are sensitive to the TBR of which value is even smaller than 1 m^2 K/GW.[7,10] As an example,

TABLE I. Techniques for TBR measurement at small scale and their comparisons. T, temperature; C_v, heat capacity; κ_S, substrate thermal conductivity.

	Measurement method	Accuracy of T detection	Sensitivity to TBR	Measurement range	Requirements
Optical	Transient thermoreflectance	High	High	Large $\geq 1\ m^2K/GW$	Known C_v and κ_S
	Raman spectroscopy	Low	High	Moderate $\geq 10\ m^2K/GW$	Transparent
Electrical	Steady-state	High	Moderate	Moderate $> 10\ m^2\ K/GW$	For metal/dielectric interface
	3ω Conventional design	Ultra-high	Moderate	Moderate $\geq 10\ m^2\ K/GW$	Known κ_S
	Two-sensor 3ω–2ω	Ultra-high	Moderate (>conventional)	Moderate (>conventional)	Known C_v

Cheng et al.[15] measured the TBR between the GaN layer and the diamond substrate, of which value is approximately $5\ m^2\ K/GW$. It is noted that to derive the target thermal properties in TTR experiments generally requires a multiple-parameter fitting process and thus a relatively complicated measurement errors analysis.[17,18] Raman spectroscopy method is another optical technique that can probe the thermal properties of nanomaterials, especially for atomically thin 2D flakes.[19,20] Also, it is capable of measuring the TBR between transparent films. Pomeroy et al.[4] measured the TBR between the GaN layer and the diamond substrate of a practical high electron mobility transistor using the Raman method. Since Raman technique can directly detect the temperature difference across the contacted transparent films, its measurement signals are very sensitive to TBR. However, in Raman experiments, temperature changes are derived from Raman shifts, which exhibit a relatively poor accuracy of temperature measurement in some cases; thus, a large temperature difference across interface is usually required to guarantee the measurement precision.[21]

Electrical techniques, which generally use metal strips fabricated on the dielectric film to locally heat the sample surface and detect the corresponding temperature response, are also applied to characterize TBR at a small scale.[22–28] Swartz and Pohl[22] proposed a steady-state electrical method to probe the TBR between a metal strip and a dielectric substrate by fabricating two parallel metal thermometers with a 2-μm-wide gap between them on the sample surface. A direct current (DC) was used to generate Joule heating within one of the two thermometers. The temperature changes of both thermometers, which can derive the temperature difference across the interface based on the time-independent heat diffusion equation, were measured by detecting the electrical resistance variations using the four-probe method.

As the representative of electrical techniques for thermal properties measurement, 3ω method is another important approach to probe the TBR between the thin film and the substrate, especially for oxide nanofilms on semiconductors.[5,25–27] In the conventional design of 3ω method, the thermal response within the metal heater is measured as a function of the thickness of the thin film to separate the contributions from the interface and the thin film. The modulated frequency of electrical heating is below 100 kHz in general;[7] thus, when compared to TTR methods, the thermal penetration length of the 3ω method becomes larger, and the thermal response is not that sensitive to TBR. The conventional 3ω method is applicable for measuring TBR of relatively large value (generally no less than $10\ m^2\ K/GW$), requiring a high-thermal-conductivity substrate.[7] In the conventional design, the two-dimensional (2D) transient heat diffusion model is generally used to derive the target parameters from the measured thermal response[27,29] In fact, this assumption of 2D heat conduction could lead to significant errors in some circumstances,[29] which requires a careful clarity to guarantee measurement accuracy. Moreover, to derive the value of TBR, the thermal conductivity of the substrate must be known in advance. Researchers[25,27] sometimes assume its value according to references, which is highly possible to deviate from its actual value. For instance, although the thermal conductivities of bulk silicon (Si) substrates have been extensively studied, it is not easy to estimate the exact value of a specific Si substrate's thermal conductivity, since the values of Si substrates can vary within a range from approximately 70 to 160 W/m K[30] due to different doping gradients as well as concentrations and fabrication conditions.

Here, a careful analysis on the deficiencies of the conventional 3ω method for probing the TBR between the thin film and the substrate is given in supplementary material S1 and S2. Three major drawbacks that greatly affect the accuracy of the TBR measurement in the conventional approach are identified by the sensitivity analysis: (i) the non-reality of generally used 2D heat conduction model, (ii) the assumption that the thermal resistances of different parts are combined in series, and (iii) the uncertainty of estimated substrate thermal conductivity. Importantly, it is found that the heater should be wide enough to fulfill the assumption that the thermal resistances of different parts are combined in series, but the increase in heater width can intensify the error of TBR caused by the estimation uncertainty of substrate thermal conductivity, which greatly limits its utilization for probing TBR especially when the thermal conductivity of the substrate is not that high.

In summary, the optical methods are generally more sensitive to TBR when compared to the electrical ones and thus can characterize the TBRs of lower values; by contrast, the electrical techniques (mainly the 3ω method) are easily operable and compatible with the measurement of other electric properties. However, there are three major deficiencies of the conventional 3ω method for probing TBR. In order to address them, we here propose a two-sensor 3ω-2ω method with a novel experimental procedure design, which can obtain the values of thin film's thermal conductivity, substrate thermal conductivity, and TBR step by step, and thus largely improve the measurement accuracy and range of TBR. As a verification, the present method is employed to measure the TBRs between amorphous alumina (Al_2O_3) nanofilm and Si as well as SiC substrates at room temperature.

II. TWO-SENSOR 3ω-2ω METHOD

The configuration of the two-sensor 3ω-2ω method is illustrated in Fig. 1. Two parallel metal sensors are fabricated, with one of them being wide and the other being narrow. Three steps are designed to derive the values of thin film's thermal conductivity, substrate thermal conductivity, and TBR separately. For evaluating the present method, a 3D model is built in commercial software (ANSYS), and FEM simulations are conducted. Details about the model settings can be found in supplementary material S3. In addition, note that the present design is to handle the isotropic materials. For the anisotropic materials, more sensors may need to be used, which requires more investigations in the future work.

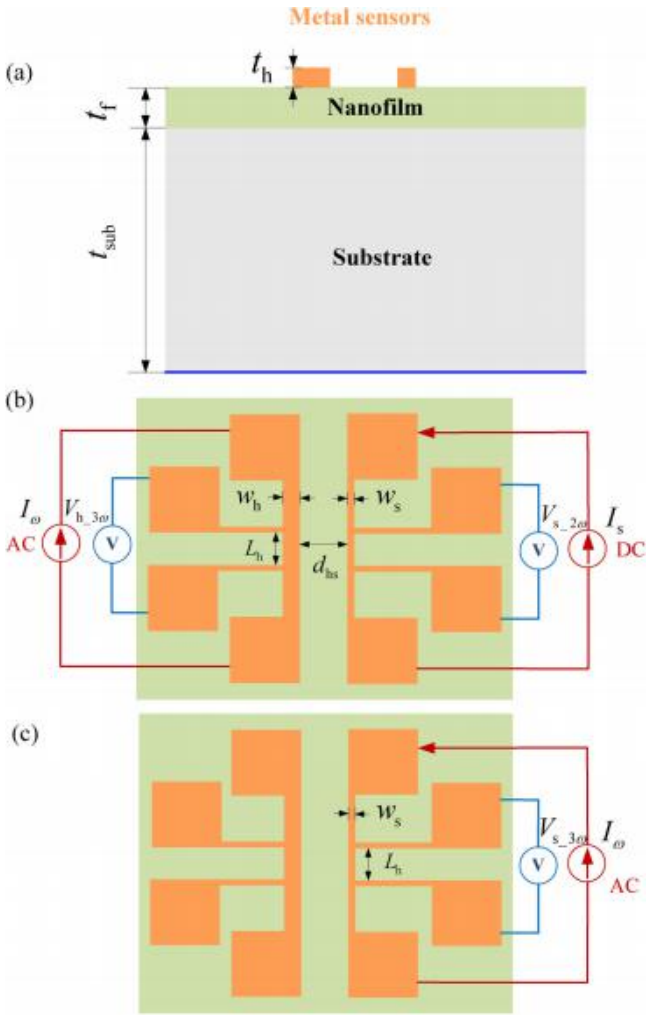

FIG. 1. Schematics of two-sensor 3ω–2ω method: (a) side view; (b) top view with the measurement circuit for steps 1 and 2; and (c) top view with the measurement circuit for step 3.

Step 1: Obtain the value of thin film's thermal conductivity from the variation of wide sensor's 3ω thermal response with the varied thickness of thin film, as an AC (I_ω) flows through the wide sensor.

When the thermal conductivity of the thin film (κ_{f0}) is not well known, we should measure it at the first step. An AC (I_ω) flows through the wide sensor, and its 3ω voltage signals ($V_{h\_3\omega}$) are measured to derive the thermal response ($\Delta T_{h\_3\omega}$),[28]

$$\Delta T_{h\_3\omega} = 2\frac{V_{h\_3\omega}}{I_\omega R_{eh}\beta_h}, \tag{1}$$

where β_h and R_{eh} are the TCR (temperature coefficient of resistance) and electrical resistance of the wide sensor. An effective thermal resistance, corresponding to the 3ω voltage signal of wide sensor, is given by

$$R_{h\_3\omega} = A_h\frac{\Delta T_{h\_3\omega}}{P} = A_h\frac{\Delta T_{h\_3\omega}}{I_\omega^2 R_{eh}}, \tag{2}$$

where P is heating power and A_h is heating area.

As the sensor is wide enough, the heat conduction within nanofilm is approximately one-dimensional, and we have

$$R_{h\_3\omega} = \frac{t_f}{\kappa_{f0}} + R_I + R_s \tag{3}$$

in which t_f is the thickness of the thin film, and R_I and R_s are the thermal resistances resulted from the interfaces and the substrate, respectively. Therefore, the same as the conventional 3ω method, the mostly straight-forwarding way to derive the value of κ_{f0} is to measure the thermal response changes for the thin films of different thickness, in terms of Eq. (3), as long as κ_{f0} does not significantly vary with the thickness, such as in the cases of amorphous oxides[31] and complex crystals of low thermal conductivity.[32]

Note that the geometrical parameters of wide sensor should be carefully designed to reduce the relative deviation of κ_{f0}.[28] Here, the method of Box–Behnken design with ANOVA (analysis of variance)[33] is utilized for the senor's geometrical parameters design (see details in supplementary material S4). According to the results of ANOVA, a sensor width equal to 40 μm can guarantee the absolute relative deviation of κ_{f0} being less than 5%, as κ_{f0} ranges from 0.5 to 2.5 W/m K (the range of κ_{f0} here is set in terms of that of amorphous oxides' thermal conductivity, which will be measured in Sec. III).

Step 2: Obtain the value of substrate thermal conductivity from the narrow sensor's 2ω thermal response, with the AC (I_ω) flowing through the wide sensor.

We will derive the value of substrate thermal conductivity (κ_s) from the narrow sensor's 2ω thermal response, when the AC for heating is flowing through the wide sensor. The 2ω voltage signals ($V_{s\_2\omega}$) are detected to obtain the thermal response ($\Delta T_{s\_2\omega}$) of

narrow sensor,

$$\Delta T_{s\_2\omega} = \frac{\sqrt{2}V_{s\_2\omega}}{I_s R_{es}\beta_s}, \quad (4)$$

in which β_s and R_{es} are the TCR and electrical resistance of the narrow sensor, and I_s is a DC flowing through the narrow sensor. In this case, an effective thermal resistance, corresponding to the 2ω voltage signal of narrow sensor, is calculated as

$$R_{s\_2\omega} = A_h \frac{\Delta T_{s\_2\omega}}{P} = A_h \frac{\Delta T_{s\_2\omega}}{I_\omega^2 R_{eh}}; \quad (5)$$

Then, κ_s's value will be derived by a non-linear fitting process between the measured and simulated values of $R_{s\_2\omega}$. To avoid the deficiencies of the 2D model, a 3D FEM-simulation based on the heat diffusion model is utilized to obtain the simulated value, which requires to input the values of several parameters, including the thermal conductivities and heat capacities of the thin film and sensors' metal, the heat capacity of substrate, and the TBR. The thin film's thermal conductivity has been derived at the first step, while the heat capacities can be found in the dataset. The key issue is that we need to estimate the value of TBR in advance, and the errors caused by this estimation are clarified using the sensitivity analysis.

To evaluate the measurement accuracy of substrate thermal conductivity, we calculate the sensitivity of κ_s with respect to $R_{s\_2\omega}$, which is denoted by $s_{\kappa_s\_R_{s2\omega}}$ and calculated in the same manner as $s_{R_I\_\kappa_s}$. As shown in Fig. 2(a), the sensitivity, $s_{\kappa_s\_R_{s2\omega}}$, is approximately 1.0, despite the variations of setting parameters, including the heating frequency (ω), the sensor's width (w_h), etc. For comparison, the sensitivity of κ_s with respect to $R_{h\_3\omega}$ (i.e.,$s_{\kappa_s\_R_{h3\omega}}$) is calculated; it is found that $s_{\kappa_s\_R_{h3\omega}}$ is larger than 1 and significantly increases with the increasing κ_s and has a strong dependence on the setting parameters' variations. Thus, we use $R_{s\_2\omega}$ to derive the value of κ_s. Moreover, since the measurement uncertainty of effective thermal resistances can be controlled under 5% in practice, the error of κ_s caused by the measurement of $R_{s\_2\omega}$ is considerably small (less than 5%).

Furthermore, the sensitivities of κ_s with respect to κ_{f0}, R_I, as well as heat capacities are calculated to clarify their influence. According to Fig. 2(b), the sensitivities for κ_{f0} (low as 0.5 W/m K), R_I (up to 200 m^2K/GW), C_{Vm} (heat capacity of the metal), and C_{Vf} (heat capacity of the thin film) are much lower than 0.05, which means that an uncertainty of these quantities equal to 100% will merely cause a relative deviation of κ_f much less than 5%. Thus, the errors resulted from their estimations could be negligible. In fact, what should be concerned about is the estimation of C_{Vs} (heat capacity of the substrate). The sensitivity for C_{Vs} increases with the decreasing κ_s and reaches approximately 0.2 with κ_s equal to 30 W/m K. Fortunately, compared to thermal conductivity, heat capacities of bulk materials generally do not vary significantly and can be readily measured using differential scanning calorimetry (DSC).[34]

Therefore, the errors caused by the estimation uncertainties of thermal conductivities and heat capacities of the thin film and sensors' metal, the heat capacity of substrate, and the TBR can be well controlled, with a rough estimation of these quantities in the reasonable range.

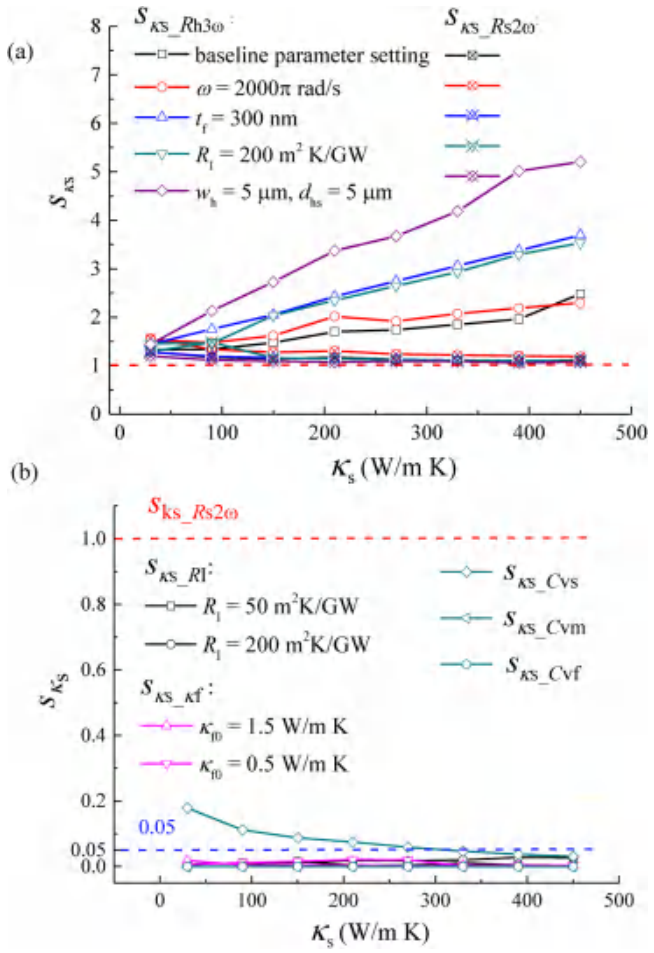

FIG. 2. (a) Sensitivities of substrate thermal conductivity (κ_s) with respect to the measured effective thermal resistances ($R_{h\_3\omega}$ and $R_{s\_2\omega}$), and the baseline parameter setting is w_h ¼ 40 μm, d_{hs} ¼ 10 μm, w_s ¼ 5 μm, ω ¼ 500 πrad/s, t_f ¼ 50 nm, R_I ¼ 50 m^2K/GW, and κ_{f0} ¼ 1:5 W/m K. (b) Sensitivities of κ_s with respect to various parameters, including TBR (R_I), thin film's thermal conductivity (κ_{f0}), and heat capacities (C_{Vs} for the substrate, C_{Vm} for the metal, and C_{Vf} for the thin film).

Step 3: Obtain the value of the TBR from the narrow sensor's 3ω thermal response, with the AC (I_ω) flowing through the narrow sensor.

An AC (I_ω) is connected into the narrow sensor, and the value of TBR will be obtained from its 3ω thermal response ($\Delta T_{s\_3\omega}$). $\Delta T_{s\_3\omega}$ is derived from the 3ω voltage signals ($V_{s\_3\omega}$) of the narrow sensor,

$$\Delta T_{s\_3\omega} = 2\frac{V_{s\_3\omega}}{I_\omega R_{es}\beta_s}; \quad (6)$$

The effective thermal resistance corresponding to $V_{s\_3\omega}$ is calculated as

$$R_{s\_3\omega} = A_h \frac{\Delta T_{s\_3\omega}}{P} = A_h \frac{\Delta T_{s\_3\omega}}{I_\omega^2 R_{es}}; \quad (7)$$

Then, a non-linear fitting process between the measured and simulated values of $R_{s\_3\omega}$ will give the value of TBR. A 3D FEM-simulation, with the input of κ_{f0} and κ_s obtained at steps 1 and 2, is used to produce the simulated values.

Note that a special attention should be paid to the actual meaning of TBR, which depends on the model setting in FEM-simulation. In the experiments of conventional 3ω method, the TBR between the metal electrode and the dielectric thin film is frequently neglected.[26,27] This assumption is plausible, when the value of TBR between the metal electrode and the dielectric thin film is comparably small. In this case, the derived TBR becomes an effective value involving the contributions from both metal/dielectric and dielectric/substrate interfaces, which might approximate the exact value of the dielectric/substrate interface. Following the conventional 3ω method, we can obtain such an effective TBR ($R_{I\_m/ox/s}$) value from $R_{s\_3\omega}$, with setting the TBR of the metal/dielectric interface ($R_{I\_m/ox}$) to 0 in the FEM-simulation.

A sensitivity analysis of $R_{I\_m/ox/s}$ is conducted to evaluate its measurement accuracy. According to Fig. 3(a), in the case of baseline parameter setting where $w_s = 5\,\mu m$, $\omega = 500\,\pi rad/s$, $t_f = 50$ nm, $\kappa_s = 150$ W/m K, and $\kappa_{f0} = 1.5$ W/m K, the sensitivity of $R_{I\_m/ox/s}$ with respect to $R_{s\_3\omega}$ ($s_{R_I\_R_{s3\omega}}$) is approximately 3, with $R_{I\_m/ox/s}$ equals to 50 m^2K/GW; thus, a measurement uncertainty equal to 5% will cause the relative error of TBR being approximately 15%. Moreover, $s_{R_I\_R_{s3\omega}}$ sharply decreases with the increasing TBR. A reduction in κ_s, an increase in w_h, or an increase in t_f can lead to an increase in $s_{R_I\_R_{s3\omega}}$, while the variation of heating frequency (ω) will not significantly affect it. Figure 3(b) shows the sensitivities of $R_{I\_m/ox/s}$ with respect to κ_{f0} and κ_s, which are denoted by $s_{R_I\_\kappa_{f0}}$ and $s_{R_I\_\kappa_s}$, respectively. Both these sensitivities significantly decrease with the increasing $R_{I\_m/ox/s}$. $s_{R_I\_\kappa_{f0}}$ increases with decreasing κ_{f0}; also, $s_{R_I\_\kappa_s}$ increases with the reduction in κ_s. Therefore, to guarantee the measurement accuracy of TBR, it is really important to accurately measure κ_{f0} and κ_s, especially when their values are not that high.

Nevertheless, in some cases where the TBR of the metal/dielectric interface is comparable to that of the dielectric/substrate interface, it is needed to separate $R_{I\_m/ox}$ from $R_{I\_m/ox/s}$. Some researchers[16,25] might choose to estimate the value of $R_{I\_m/ox}$ according to references, which may result in considerable errors as the estimation of substrate thermal conductivity. In fact, a better option should be obtaining $R_{I\_m/ox}$ and $R_{I\_ox/s}$ simultaneously in the fitting processes. The TTR techniques are capable of this, while it can be somewhat difficult in the conventional 3ω method.

Here, our simulations reveal that these two TBRs are distinguishable when the heater is not that wide, due to the considerable difference between their contact areas. To demonstrate this point, we keep the summation of $R_{I\_m/ox}$ and $R_{I\_ox/s}$ unchanged, but alter the ratio between them. As shown in Fig. 4, the heater's effective thermal resistance increases with the increasing proportion of $R_{I\_m/ox}$. This indicates that the TBR of the metal/dielectric interface has a more profound influence on the heater's effective thermal resistance, owing to its smaller contact area. Such property enables us to separate these two TBRs by varying the contact area (i.e., the heater's width). Note that the effective TBR derived by setting $R_{I\_m/ox} = 0$ in simulations will not be the summation of $R_{I\_m/ox}$ and $R_{I\_ox/s}$, since each TBR has different influence on the measured effective thermal resistance.

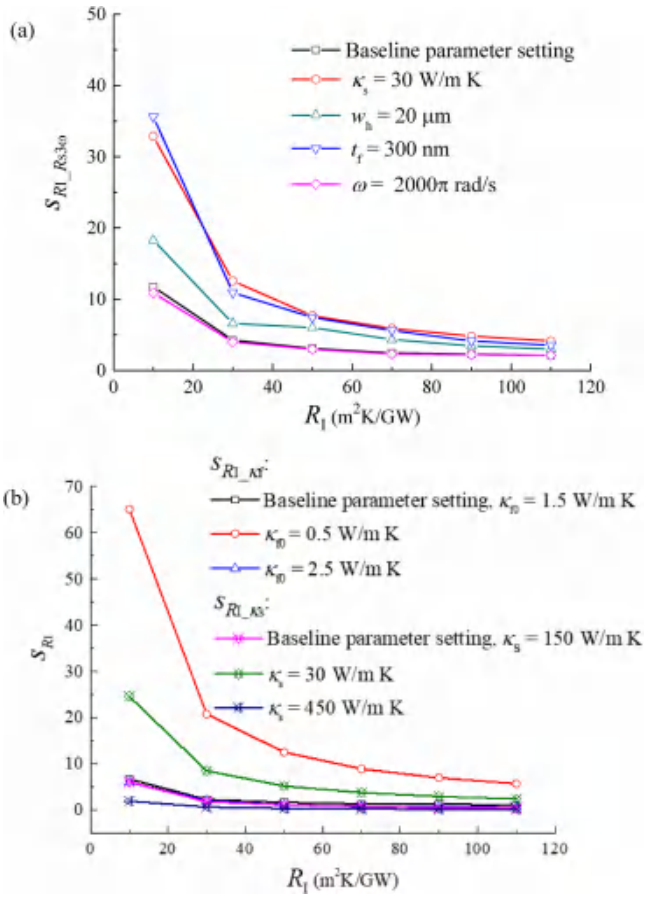

FIG. 3. Sensitivities of TBR (R_I), and the baseline parameter setting is $w_s = 5\,\mu m$, $\omega = 500\,\pi rad/s$, $t_f = 50$ nm, $\kappa_s = 150$ W/m K, and $\kappa_{f0} = 1.5$ W/m K. (a) Sensitivity of R_I with respect to the measured effective thermal resistance ($R_{s\_3\omega}$): $s_{R_I\_R_{s3\omega}}$. (b) Sensitivities of R_I with respect to the thin film's thermal conductivity (κ_{f0}) and substrate thermal conductivity (κ_s): $s_{R_I\_\kappa_{f0}}$ and $s_{R_I\_\kappa_s}$.

III. EXPERIMENTS

To verify the applicability of the two-sensor 3ω-2ω method, it is employed to measure the TBRs between Al_2O_3 nanofilm and Si as well as SiC substrates at room temperature. The first set of samples are Al_2O_3 nanofilms (grown by ALD methods) on single crystal Si (450 μm-thick); the thicknesses of Al_2O_3 nanofilms are 54, 208, and 311 nm. The second sample is the Al_2O_3 nanofilm

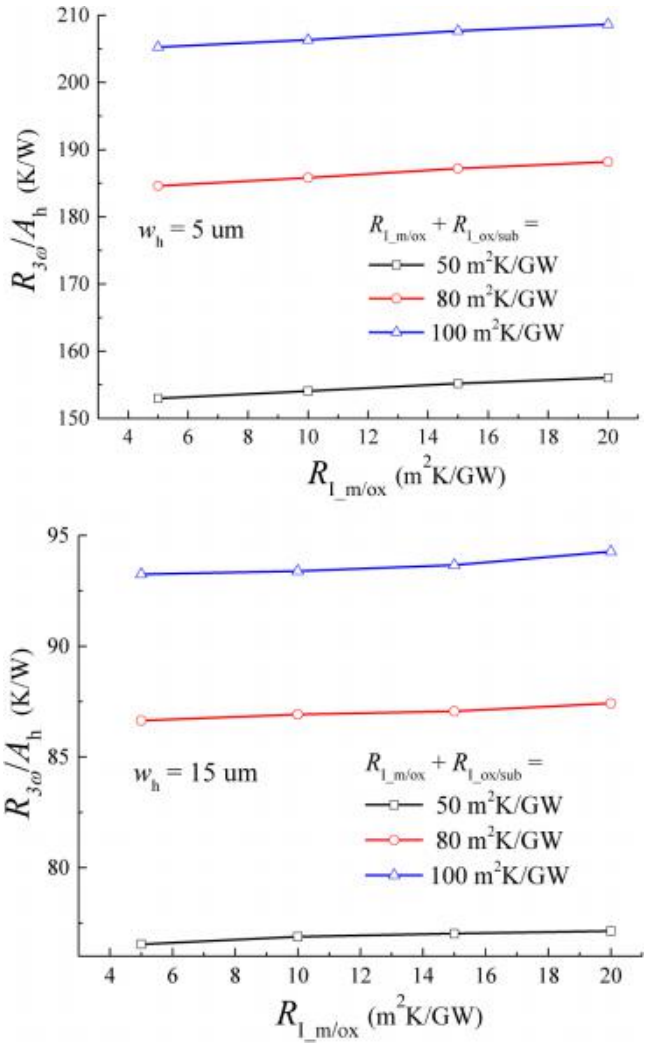

FIG. 4. The effective thermal resistance of heater vs the TBR of the metal/dielectric interface, with the summation of the TBRs of metal/dielectric and dielectric/substrate interfaces unchanged.

(51 nm-thick) on single crystal 4H-SiC (350 μm-thick). The samples were brought from the company: we chose materials and designed the patterns of metal sensors, while the company conducted material growth and metal sensors' fabrication. During the fabrication, the standard cleaning processes were conducted using DI water, acetone, etc., to clean these wafers; the standard lithography process was conducted to define the sensors' patterns, and the metal sensors (10 nm Cr/100 nm Pt) were fabricated by sputtering. Figure 5 illustrates the microscope photos of metal sensors. There are two sets of sensors on the sample of the Si substrate: as for set #1, the width of the wide sensor (w_h) is designed to be 40 μm, and the width of the narrow sensor is designed to be 5 μm, with the gap between them designed to be 10 μm; set #2 is fabricated for separating the TBR of the dielectric/metal interface and that of the dielectric/substrate interface, and merely its wide sensor of width designed to be 15 μm is used in our experiments. By contrast, for the sample of the SiC substrate, two narrow sensors with width equal to 5 μm and a 5 μm gap between them are designed. Moreover, the half whole length of the wide sensor is 400 μm, while the half length of its central part is only 75 μm. The half length of the narrow sensor is also 75 μm. Therefore, what we measure in experiments are the temperature oscillations averaged over the central part, and the 3D FEM simulations f or nonlinear fitting are conducted accordingly (in supplementary material S6). After fabrication, we remeasured the sensors' width using microscopy. Their exact dimensions are summarized in Table II (ore measurement details in supplementary material S5).

In terms of the procedures stated above, the thermal conductivity of Al_2O_3 is measured using set #1's wide sensor on the sample of the Si substrate. Subsequently, the values of the substrate thermal conductivity and the effective TBR ($R_{I\_m/ox/s}$) for the sample of the Si substrate are derived from $R_{s\_2\omega}$ and $R_{s\_3\omega}$ of set #1, respectively. Furthermore, the wide sensor's effective thermal resistance of set #2 ($R^{\#2}_{h\_3\omega}$) is measured; then, the TBRs of metal/Al_2O_3 and Al_2O_3/Si interfaces ($R_{I\_m/ox}$ and $R_{I\_ox/Si}$) can be obtained by the combination of $R_{s\_3\omega}$ and $R^{\#2}_{h\_3\omega}$. As for the sample of the SiC substrate, it is plausible to assume that its nanofilm has the same thermal conductivity value as that in the sample of the Si substrate, since amorphous Al_2O_3's thermal conductivity is generally stable and independent of thickness. Thus, step 1 can be skipped, and the width of the sensor is not needed to be that wide to suppress the relative deviation of κ_f. Two narrow sensors are fabricated on the sample of the SiC substrate. An AC is connected into one of the narrow sensors for heating, while a DC is flowing through the other sensor. In this way, we can measure $R_{s\_2\omega}$ and $R_{s\_3\omega}$ to derive the values of substrate thermal conductivity and the effective TBR in a single measurement. Moreover, since the TBR of the metal/Al_2O_3 interface has already been obtained in the measurement of the sample of the Si substrate, the TBR of Al_2O_3/SiC interface can be readily derived from $R_{s\_3\omega}$ (more details of data processing and error analysis in supplementary material S6–S8).

Our experimental results are summarized in Table III. The intrinsic thermal conductivity of amorphous Al_2O_3 at room temperature is measured to be 1.72 ± 0.09 W/m K, which is within the range (1.3–2.6 W/m K) of previous experiments of amorphous ALD-grown Al_2O_3.[16] The measured thermal conductivity values of both substrates (κ_{Si} ¼ 149:9 + 5:2 W/m K, κ_{SiC} ¼ 393:9 + 12:5 W/m K) are in good agreements with those reported in literatures.[35,36]

Regarding the TBRs, Fig. 6 compares our experimental data to the previous measurements and the DMM (diffuse mismatch model)-based predictions (the calculation details of DMM can be found in supplementary material S9). Scott et al.[16] measured the TBR of the Al/Al_2O_3/Si interface equal to approximately 6 m² K/GW, which is significantly lower than our measured value (37:2 + 5:1 m²K/GW) for the Pt/Cr/Al_2O_3/Si interface. This deviation might result from the metal/Al_2O_3 interface of which TBR value can range from approximately 5 to 20 m² K/GW.[37] For comparison, this TBR is also derived using the traditional method (details in supplementary material S5). The value of $R_{I\_m/ox/s}$ is

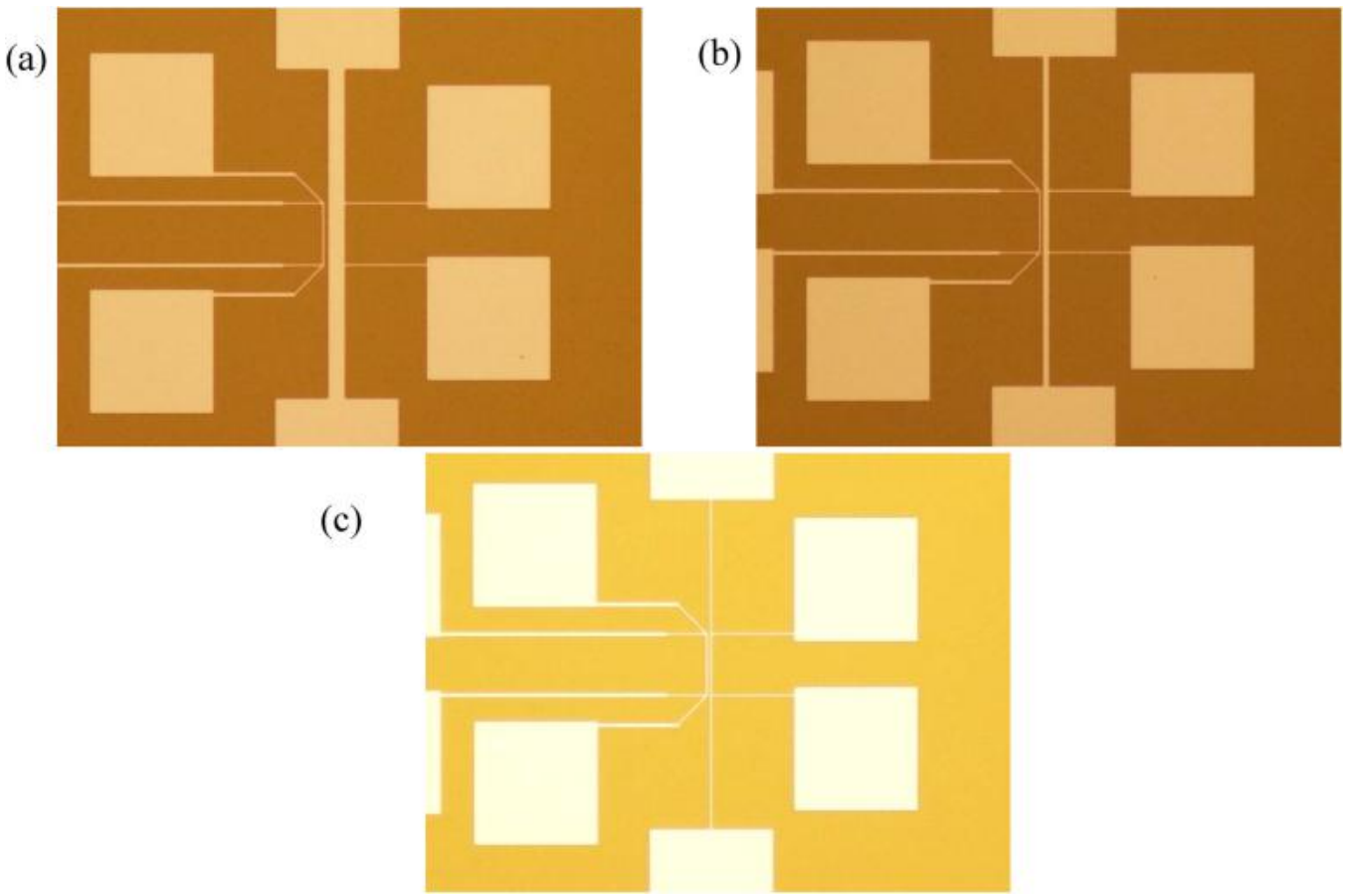

FIG. 5. Microscope photos of metal sensors (50×): (a) the sensors on the sample of the Si substrate; (b) the sensors on the sample of the SiC substrate.

found to be $40.7 \pm 12.2\ m^2$ K/GW; its relative error can reach about 30.0%, due to the error propagation from substrate thermal conductivity. By contrast, the relative error of $R_{I\_m/ox/s}$ obtained by the two-sensor method is only approximately 14.5%. Actually, our measured effective TBRs are close to those of Au/Cr/SiO_2/Si and Au/Cr/SiO_2/SiC interfaces reported by Deng et al.[27] Moreover, the TBR of the Pt/Cr/Al_2O_3 interface in the present work is found to be 15:8 + 1:1 m^2K/GW, which lies in the range of TBR of metal/Al_2O_3 interface (5–20 m^2 K/GW) reported in references.[37] The TBR between the metal and the dielectric is supposed to be highly dependent on the surface and fabrication conditions; thus, it is not surprise that the TBR's value can vary within a considerably large range. After excluding the TBR of Pt/Cr/Al_2O_3 interface from the effective TBRs, the TBR of Al_2O_3/Si interface becomes 19:2 + 3:3 m^2K/GW, while that of Al_2O_3/SiC interface is 55:7 + 4:5 m^2K/GW. Deng et al.[27] also identified the similar phenomenon that the TBR value between oxides and SiC should be higher than that between oxides and Si, which could be attributed to the high density of interfacial defects between SiC and its native oxide.

TABLE II. Exact geometrical dimensions of sensors.

Sample	w_h	w_s	d_{hs}
Si #1	41.5 μm	5.5 μm	8.9 μm
Si #2	15.5 μm	N/A	N/A
SiC	5.6 μm	5.5 μm	5.0 μm

TABLE III. Experimental results in the present work.

Substrate	κ_{f0} (W/m K)	κ_s (W/m K)	$R_{I\_m/ox/s}$ (m^2 K/GW)	$R_{I\_m/ox}$ (m^2 K/GW)	$R_{I\_ox/s}$ (m^2 K/GW)
Si	1.72 ± 0.09	149.9 ± 5.4	37.2 ± 5.4	15.8 ± 1.1	19.2 ± 3.3
SiC	1.72 ± 0.09	393.9 ± 12.5	74.5 ± 5.9	15.8 ± 1.1	55.7 ± 4.5

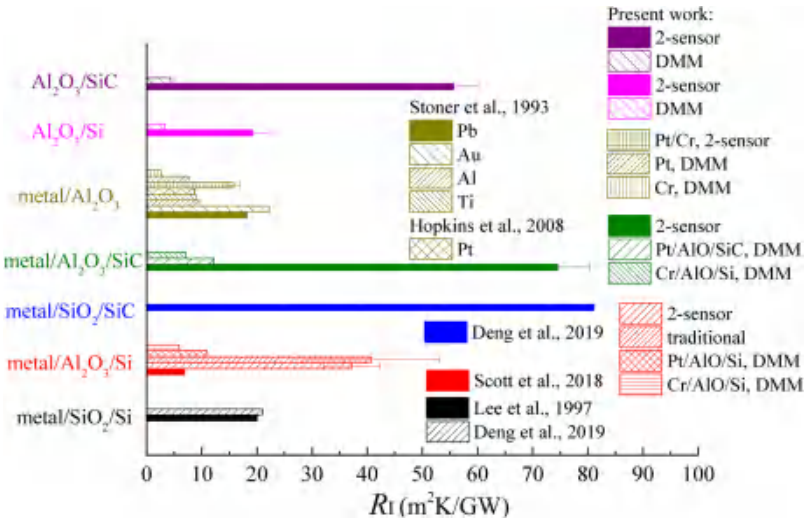

FIG. 6. Comparisons of TBRs between present data, DMM-based predictions, and previous measurements.

Lastly, the TBRs calculated by DMM range from 2 to 8 m^2K/GW, which are smaller than the measured values that are within the range from 10 to 80 m^2K/GW. In fact, the DMM only considers the phonon properties' difference between the contacting materials but neglects the impact of defects near the interface that highly depends on fabrication conditions and can significantly vary from one sample to another sample. Therefore, the DMM-based predictions can deviate from the experimental results, and the measured TBRs can also be different even for the identical contacting materials. For instance, Hopkins et al.[38] used the TTR method to measure the TBRs of the interfaces between c-Al_2O_3 (sapphire) and metals, and the experimental results are close to the DMM-based predictions; by contrast, the TBR for a-Al_2O_3/Pt interface measured by Cappella et al.[39] was found to be approximately 100 m^2K/GW, which is two order-magnitude larger than the model's calculation. Particularly in our case, different from the TTR method where the metal transducer is directly deposited on the substrate, to obtain the designed sensor configurations in the electrical methods generally requires a serial of processes, including photoresist coating, lithography, etching, etc., which is possible to introduce interfacial defects. The interfacial defect density in our experiments is expected to be higher than that in Hopkins et al.'s case,[38] and this may lead to larger TBR values compared to the DMM-based predictions.

IV. CONCLUSIONS

In the present work, we propose a two-sensor 3ω-2ω method combined with FEM-simulation and inverse-problem method to address the deficiencies in the conventional 3ω method. Two parallel metal sensors are fabricated, with one of them being wide and the other being narrow. The rising temperatures of these two sensors are measured by detecting the 3ω and 2ω signals, respectively. A novel experimental procedure is designed to derive the values of thin film's thermal conductivity, substrate thermal conductivity, and TBR separately.

To verify the applicability of our method, it is applied to probe the TBRs between Al_2O_3 nanofilm and Si and SiC substrates at room temperature. The thermal conductivities of amorphous Al_2O_3 nanofilms, Si, and SiC substrates are measured to be 1.72 ± 0.09, 149:9 + 5:2, and 393:9 + 12:5 W/m K, respectively, which are in good agreement with the previous measurements. Moreover, the effective TBR values involving the contributions from both metal/dielectric and dielectric/substrate interfaces are fitted to be 37:2 + 5:1 and 74:5 + 5:9 m^2K/GW for the Pt/Cr/Al_2O_3/Si and Pt/Cr/Al_2O_3/SiC interfaces, respectively. After excluding the TBR of metal/Al_2O_3 interface that is measured to be 15:8 + 1:1 m^2K/GW, the TBRs of Al_2O_3/Si and Al_2O_3/SiC interfaces become 19:2 + 3:3 and 55:7 + 4:5 m^2K/GW, respectively.

The present scheme provides an alternative way that can probe the thermal conductivities and TBR simultaneously and have better measurement accuracy compared to the conventional 3ω method. Additionally, the increase in experimental cost is limited for the present scheme: no other instruments are needed when compared to the conventional 3ω method; the added cost for device fabrication is also acceptable, since the metal sensors with various widths and configurations can be fabricated during one standard lithography process. Therefore, the present scheme will be helpful for the experimental study of interfacial thermal transport.

SUPPLEMENTARY MATERIAL

See the supplementary material for the sensitivity analysis of conventional 3ω method (S1 and S2), the simulations details for two-sensor 3ω–2ω method (S3), the details of Box–Behnken design with ANOVA (S4), the details of measurement and nonlinear fitting (S5 and S6), the clarification for the influence of heating frequency on the experiment results (S7), error analysis (S8), and the details of DMM (S9).

ACKNOWLEDGMENTS

This work was financially supported by the National Natural Science Foundation of China (NNSFC; Nos. 51906121, 51825601, and U20A20301), the National Key R&D Program of China (No. 2016YFB0600100), and the Tsinghua National Laboratory for Information Science and Technology of China (TNList).

DATA AVAILABILITY

The data that support the findings of this study are available from the corresponding author upon reasonable request.

REFERENCES

[1]A. L. Moore and L. Shi, "Emerging challenges and materials for thermal management of electronics," Mater. Today 17(4), 163–174 (2014).
[2]Y.-C. Hua and B.-Y. Cao, "Study of phononic thermal transport across nanostructured interfaces using phonon Monte Carlo method," Int. J. Heat Mass Transfer 154, 119762 (2020).
[3]J. Cho, E. Bozorg-Grayeli, D. H. Altman, M. Asheghi, and K. E. Goodson, "Low thermal resistances at GaN–SiC interfaces for HEMT technology," IEEE Electron Device Lett. 33(3), 378–380 (2012).
[4]J. W. Pomeroy, M. Bernardoni, D. C. Dumka, D. M. Fanning, and M. Kuball, "Low thermal resistance GaN-on-diamond transistors characterized by three-dimensional Raman thermography mapping," Appl. Phys. Lett. 104(8), 083513 (2014).
[5]G. Bulman, P. Barletta, J. Lewis, N. Baldasaro, M. Manno, A. Bar-Cohen, and B. Yang, "Superlattice-based thin-film thermoelectric modules with high cooling fluxes," Nat. Commun. 7, 10302 (2016).
[6]K. M. Shahil and A. A. Balandin, "Graphene-multilayer graphene nanocomposites as highly efficient thermal interface materials," Nano Lett. 12(2), 861–867 (2012).
[7]C. Monachon, L. Weber, and C. Dames, "Thermal boundary conductance: A materials science perspective," Annu. Rev. Mater. Res. 46(1), 433–463 (2016).
[8]A. Giri and P. E. Hopkins, "A review of experimental and computational advances in thermal boundary conductance and nanoscale thermal transport across solid interfaces," Adv. Funct. Mater. 30(8), 1903857 (2019).
[9]Y.-C. Hua and B.-Y. Cao, "Interface-based two-way tuning of the in-plane thermal transport in nanofilms," J. Appl. Phys. 123(11), 114304 (2018).
[10]P. Jiang, X. Qian, and R. Yang, "Tutorial: Time-domain thermoreflectance (TDTR) for thermal property characterization of bulk and thin film materials,' J. Appl. Phys. 124, 161103 (2018).
[11]R. Cheaito, J. T. Gaskins, M. E. Caplan, B. F. Donovan, B. M. Foley, A. Giri, J. C. Duda, C. J. Szwejkowski, C. Constantin, H. J. Brown-Shaklee, J. F. Ihlefeld, and P. E. Hopkins, "Thermal boundary conductance accumulation and interfacial phonon transmission: Measurements and theory," Phys. Rev. B 91(3), 035432 (2015).
[12]R. Garrelts, A. Marconnet, and X. Xu, "Assessment of thermal properties via nanosecond thermoreflectance method," Nanoscale Microscale Thermophys. Eng. 19(4), 245–257 (2015).
[13]G. T. Hohensee, R. B. Wilson, and D. G. Cahill, "Thermal conductance of metal-diamond interfaces at high pressure," Nat. Commun. 6, 6578 (2015).
[14]R. B. Wilson, B. A. Apgar, W.-P. Hsieh, L. W. Martin, and D. G. Cahill, "Thermal conductance of strongly bonded metal-oxide interfaces," Phys. Rev. B 91(11), 115414 (2015).
[15]Z. Cheng, F. Mu, L. Yates, T. Suga, and S. Graham, "Interfacial thermal conductance across room-temperature-bonded GaN/diamond interfaces for GaN-on-diamond devices," ACS Appl. Mater. Interfaces 12(7), 8376–8384 (2020).
[16]E. A. Scott, J. T. Gaskins, S. W. King, and P. E. Hopkins, "Thermal conductivity and thermal boundary resistance of atomic layer deposited high-k dielectric aluminum oxide, hafnium oxide, and titanium oxide thin films on silicon," APL Mater. 6(5), 058302 (2018).
[17]J. Cho, D. Francis, D. H. Altman, M. Asheghi, and K. E. Goodson, "Phonon conduction in GaN-diamond composite substrates," J. Appl. Phys. 121(5), 055105 (2017).
[18]J. Yang, E. Ziade, and A. J. Schmidt, "Uncertainty analysis of thermoreflectance measurements," Rev. Sci. Instrum. 87(1), 014901 (2016).
[19]H. Malekpour and A. A. Balandin, "Raman-based technique for measuring thermal conductivity of graphene and related materials," J. Raman Spectrosc. 49(1), 106–120 (2018).
[20]Q. Cai, D. Scullion, W. Gan, A. Falin, S. Zhang, K. Watanabe, T. Taniguchi, Y. Chen, E. J. G. Santos, and L. H. Li, "High thermal conductivity of high-quality monolayer boron nitride and its thermal expansion," Sci Adv 5(6), eaav0129 (2019).
[21]T. Beechem, L. Yates, and S. Graham, "Invited review article: Error and uncertainty in Raman thermal conductivity measurements," Rev. Sci. Instrum. 86(4), 041101 (2015).
[22]E. T. Swartz and R. O. Pohl, "Thermal resistance at interfaces," Appl. Phys. Lett. 51(26), 2200–2202 (1987).
[23]X. Li, W. Park, Y. Wang, Y. P. Chen, and X. Ruan, "Reducing interfacial thermal resistance between metal and dielectric materials by a metal interlayer," J. Appl. Phys. 125(4), 045302 (2019).
[24]Y.-C. Hua, L. Xing, L.-Y. Jiao, and B.-Y. Cao, "An electrical thermometry platform for measuring cross-plane thermal conductivity of 2D flakes on substrate," Appl. Phys. Lett. 115(12), 123102 (2019).
[25]S. M. Lee and D. G. Cahill, "Heat transport in thin dielectric films," J. Appl. Phys. 81(6), 2590–2595 (1997).
[26]Z. Wang, M. Sun, G. Yao, D. Tang, and K. Xu, "Reconstruction of thermal boundary resistance and intrinsic thermal conductivity of SiO 2-GaN-sapphire structure and temperature dependence," Int. J. Therm. Sci. 87, 178–186 (2015).
[27]S. Deng, C. Xiao, J. Yuan, D. Ma, J. Li, N. Yang, and H. He, "Thermal boundary resistance measurement and analysis across SiC/SiO_2 interface," Appl. Phys. Lett. 115(10), 101603 (2019).
[28]C. Dames, "Measuring the thermal conductivity of thin films: 3 omega and related electrothermal methods," Annu. Rev. Heat Transf. 16, 7–49 (2013).
[29]W. Jaber and P.-O. Chapuis, "Non-idealities in the 3ω method for thermal characterization in the low- and high-frequency regimes," AIP Adv. 8(4), 045111 (2018).
[30]Y. Lee and G. S. Hwang, "Mechanism of thermal conductivity suppression in doped silicon studied with nonequilibrium molecular dynamics," Phys. Rev. B 86(7), 075202 (2012).
[31]M. C. Wingert, J. Zheng, S. Kwon, and R. Chen, "Thermal transport in amorphous materials: A review," Semicond. Sci. Technol. 31(11), 113003 (2016).
[32]M. Beekman and D. G. Cahill, "Inorganic crystals with glass-like and ultralow thermal conductivities," Cryst. Res. Technol. 52(10), 1700114 (2017).
[33]NIST/SEMATECH e-Handbook of Statistical Methods (NIST, 2012).
[34]P. S. Gill, S. R. Sauerbrunn, and M. Reading, "Modulated differential scanning calorimetry," J. Therm. Anal. 40(3), 931–939 (1993).
[35]M. Asheghi, M. N. Touzelbaev, K. E. Goodson, Y. K. Leung, and S. S. Wong, "Temperature-dependent thermal conductivity of single-crystal silicon layers in SOI substrates," J. Heat Transfer 120(1), 30–36 (1998).
[36]R. Wei, S. Song, K. Yang, Y. Cui, Y. Peng, X. Chen, X. Hu, and X. Xu, "Thermal conductivity of 4H-SiC single crystals," J. Appl. Phys. 113(5), 053503 (2013).
[37]R. J. Stoner and H. J. Maris, "Kapitza conductance and heat flow between solids at temperatures from 50 to 300 K," Phys. Rev. B 48(22), 16373–16387 (1993).
[38]P. E. Hopkins, P. M. Norris, and R. J. Stevens, "Influence of inelastic scattering at metal-dielectric interfaces," J. Heat Transfer 130(2), 022401 (2008).
[39]A. Cappella, J.-L. Battaglia, V. Schick, A. Kusiak, A. Lamperti, C. Wiemer, and B. Hay, "High temperature thermal conductivity of amorphous Al_2O_3Thin films grown by low temperature ALD," Adv. Eng. Mater. 15(11), 1046–1050 (2013).